# Time-lapse GPR measurement to study the imaging operator

*Jan Harry Zeeman*, Jeroen Groenenboom and Jan van der Kruk, TU Delft*

## Summary

This paper aims at improving imaging algorithms for ground penetrating radar data. Recent efforts try to achieve this by incorporating the electromagnetic vector propagation, describing the source and receiver antenna as far field point-source radiation patterns. Here, we show that a theoretically sound imaging operator can be constructed based on the response of an approximate point scatterer, including the effect of source and receiver antenna. With an automated frame we have measured a three-dimensional data set over homogeneous sand. Then we buried a scatterer at a depth of roughly a half a meter and measured the data set again. By subtracting these data sets in a time lapse manner we can roughly estimate the point scatterer response. We have compared this response with the far field point source/receiver response and show that for the real data the amplitude versus offset to the scatterer falls off much more rapidly than according to theory. The two most likely causes of this fact are the finite aperture of the antennas and the attenuation in the ground. In principle the measured data can be used to construct improved imaging operators.

## Introduction

In shallow geophysics, the GPR is widely used to characterize the subsurface. Imaging is used because raw GPR data do not adequately represent the subsurface. Imaging operators are based on a forward model and the imaging operator can not be more accurate than the forward model used. Seismic imaging methods, such as the Gazdag method, (Gazdag, 1978), or the diffraction stack, are based on the scalar acoustic wave-equation and radiation pattern. These methods do not take into account the vectorial character of the EM field. So, more sophisticated methods are developed (van der Kruk et al., 2001; Wang and Oristaglio, 2000; van der Kruk et al., 2000), based on the vectorial EM field and antenna radiation pattern. These methods are using a model based on a point source and receiver, and a homogenous halfspace. The spatial impulse response of this forward model, a diffractor, is then used to make an imaging operator. But when GPR data is measured, the antennas are in fact finite and the medium is inhomogeneous. The objective of this paper is to compare a measured measured diffraction response to a forward model impulse response based on point dipole source and receiver. This way it can be assessed whether the forward model is sufficient for migration purposes.

## Forward model

For simplicity, this deduction is limited to a point source and receiver. The linearized expression for the scattering formalism, based on the Born approximation, is given by, (de Hoop, 1995),

$$\hat{E}_r^{sct}(\boldsymbol{x}^r,\boldsymbol{x}^s,\omega) = \int_{\boldsymbol{x}'\in\mathbb{D}_{sct}} \Big[\hat{G}_{rk}^{EJ}(\boldsymbol{x}^r,\boldsymbol{x}',\omega)\hat{\chi}^{\eta}(\boldsymbol{x}',\omega) \hat{G}_{kj}^{EJ}(\boldsymbol{x}',\boldsymbol{x}^s,\omega)\hat{J}_j(\omega)\Big]dV. \quad (1)$$

The spatial dependence is split into the horizontal $x_\alpha$, $\alpha = (1,2)$, and vertical $x_3$ coordinates. For a lateral invariant background medium the Green's functions can be written as,

$$\hat{G}_{kj}^{EJ}(x_\alpha^r,x_\alpha',x_3^r,x_3',\omega) = \hat{G}_{kj}^{EJ}(x_\alpha^r-x_\alpha',x_3^r,x_3',\omega), \quad (2a)$$

$$\hat{G}_{rk}^{EJ}(x_\alpha',x_\alpha^s,x_3',x_3^s,\omega) = \hat{G}_{rk}^{EJ}(x_\alpha'-x_\alpha^s,x_3',x_3^s,\omega). \quad (2b)$$

All propagation effects of the electromagnetic field are contained within the Green's functions. It is now practical to combine these Green's functions in a two-way wave propagation kernel $\hat{\Gamma}_{rj}$, containing the Greens function from scattering media to receiver and the Greens function from source to scattering media

$$\hat{\Gamma}_{rj}(x_\alpha^r,x_3^r,x_\alpha^s,x_3^s,x_\alpha',x_3',\omega) = \hat{G}_{rk}^{EJ}(x_\alpha^r-x_\alpha',x_3^r,x_3',\omega)\hat{G}_{jk}^{EJ}(x_\alpha^s-x_\alpha',x_3^s,x_3',\omega). \quad (3)$$

This expression is valid due to the reciprocity and the shift invariance of the background medium in the lateral direction. If the measurements are on a fixed offset pattern, the following relations hold,

$$x_\alpha^s = x_\alpha^r - x_\alpha^o, \quad (4a)$$

$$x_3^s = x_3^r, \quad (4b)$$

where $x_\alpha^o$ is the *constant* horizontal offset vector. The source positions, $x_\alpha^s$ and $x_3^s$, can be eliminated from $\hat{\Gamma}_{rj}$,

$$\hat{\Gamma}_{rj}(x_\alpha^r-x_\alpha',x_3^r,x_3',\omega) = \hat{G}_{rk}^{EJ}(x_\alpha^r-x_\alpha',x_3^r,x_3',\omega) \hat{G}_{jk}^{EJ}(x_\alpha^r-x_\alpha^o-x_\alpha',x_3^r,x_3',\omega). \quad (5)$$

Substituting eq.5 in eq.1 results in,

$$\hat{E}_r^{sct}(x_\alpha^r, x_3^r, \omega) = \int_0^H \int_{x'_\alpha \in \mathbb{D}_{\alpha,sct}} \left[\hat{\Gamma}_{rj}(x_\alpha^r - x'_\alpha, x_3^r, x'_3, \omega)\hat{\chi}^\eta(x'_\alpha, x'_3, \omega)\hat{J}_j(\omega)\right] dx'_\alpha\, dx'_3. \quad (6)$$

The convolution in eq.6 in the space-domain becomes a product in the wave number domain.

$$\tilde{E}_r^{sct}(k_\alpha, x_3, \omega) = \int_0^H \tilde{\Gamma}_{rj}(k_\alpha, x_3^r, x'_3, \omega)\tilde{J}_j(\omega)\tilde{\chi}^\eta(k_\alpha, x'_3, \omega)dx'_3. \quad (7)$$

## Imaging

A migration operator can be defined as the inverse of the propagator and the wavelet. For single component imaging the summation convention is invalidated, so the subscripts are changed to capitals. Thus the migration operator is defined as

$$M(k_\alpha, x_3^r, x_3, \omega) = \left(\tilde{\Gamma}_{KM}(k_\alpha, x_3^r, x_3, \omega)\tilde{J}_M(\omega)\right)^{-1}. \quad (8)$$

$\left(\tilde{J}_M(\omega)\right)^{-1}$ corresponds to source wavelet deconvolution. Using the inverse propagation-wavelet tensor, and the imaging principle (Berkhout, 1982), the $\tilde{\chi}^\eta$ contrast at an arbitrary level, is given by

$$\tilde{\chi}^\eta(k_\alpha, x_3) = 2Re\int_{\omega_1}^{\omega_2} M(k_\alpha, x_3^r, x_3, \omega)\tilde{E}_K^{sct}(k_\alpha, x_3^r, \omega)\mathrm{d}\omega. \quad (9)$$

Eq.9 shows that the imaging operator is the inverse of the propagation kernel. Deconvolution is also part of the inverse of the propagation kernel.

## Data-driven imaging

If the scattered electric field results from a sufficient small scatterer, and the Green's functions can be assumed constant over the volume of the scatterer, the integral in eq.1 reduces to an integral over the volume ($V$) of the scatterer.

$$\hat{E}_r^{sct}(\boldsymbol{x}^r, \boldsymbol{x}^s, \omega) = \hat{G}_{rk}^{EJ}(\boldsymbol{x}^r, \boldsymbol{x}', \omega)\hat{\chi}(\omega)\hat{G}_{kj}^{EJ}(\boldsymbol{x}', \boldsymbol{x}^s, \omega)\hat{J}_j(\omega)V. \quad (10)$$

Following the same reasoning as in the forward model, the Green's functions can be contracted to a two-way wave propagation kernel $\hat{\Gamma}_{rj}$ containing the Greens function from scattering media to receiver and the Greens function from source to scattering media.

$$\hat{E}_r^{sct}(x_\alpha^r - x'_\alpha, x_3^r, x'_3, \omega) = \left(\hat{\Gamma}_{rj}(x_\alpha^r - x'_\alpha, x_3^r, x'_3, \omega)\hat{J}_j(\omega)\right)^{sct}\hat{\chi}(\omega)V. \quad (11)$$

From measurements the electric field is only know at the surface so the vertical coordinate can be replaced by a parameter. $V$ and $\hat{\chi}(\omega)$ ar constant, so eq.11 is written as,

$$\left(\hat{\Gamma}_{rj}(x_\alpha^r - x'_\alpha, x_3^r, x_3, \omega)\hat{J}_j(\omega)\right)^{sct} = \frac{1}{V.\hat{\chi}(\omega)}\hat{E}_r^{sct}(x_\alpha^r, x_3^r, \omega). \quad (12)$$

The forward operator can be based on the diffraction data itself. By tranformation to the wavenumber domain and inverting the measured data can be used as an imaging operator in eq.9. It has to be noted that the imaging operator is only valid for the same depth level as the scatterer.

## Experimental results

The data for the imaging operator has to be of high accuracy. In order to get a highly accurate positioning, an automated measuring frame was developed (figure 1). With this frame a positioning error of less than

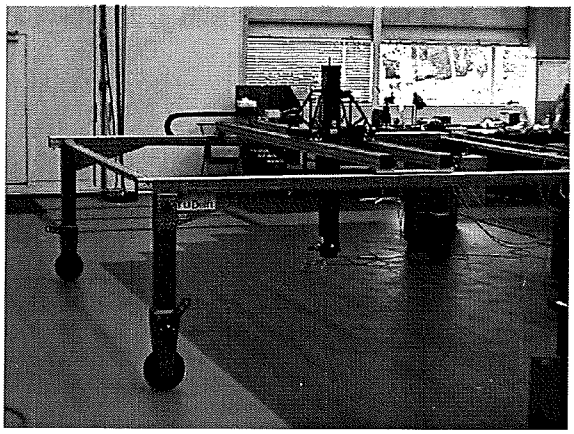

Fig. 1: The measurement frame in the laboratory, with an effective measurement size of 3 by 3 meter. Note the possibility to measure with elevated antennas as well as ground coupled antennas.

a millimeter was possible. Not only in the horizontal plane, but also in the vertical direction. A sampling interval of 2.5 cm was chosen. A broadside 900 MHz PulseEkko antenna configuration was used to acquire GPR data. The measurements were done at a controlled test site containing a sandpit with rather homogeneous sand. After realigning the data in the time domain, no

processing was done. The result can be viewed in figure 2.

After the initial measurements, a metal (aluminium) sphere with a diameter of 15cm was buried, with it's top at a depth of 55 cm. The same C-scan was measured again and a line of data is shown in figure 3. Again, the realignment of the data in the time domain was the only processing step done. Both data sets were subtracted from each other and the result can be seen in figure 4 and figure 5. Not only is the diffractor visible but also the disturbed soil resulting from the burial of the sphere. Note that the energy of the diffractor seems to be higher in the disturbed area. The soil disturbance has a greater energy than the diffraction, and can easily be muted. This is done in figure 6,

To compare this diffractor with a forward model, a theoretical diffraction pattern was calculated, using far field expressions for dipole source and receiver antennas, (Engheta and Papas, 1982), and the same spatial configuration as in the measurements. The results can be seen in figure 7. Differences with the model compared to the measured diffractor are, that the energy in the tails is less than predicted compared to the zero offset amplitude. Also, the phase shift in the tails of the data seems to be less than the modeled data. The higher energy content in the top of the diffractor under the disturbed soil is also noted in the data.

## Conclusions

A framework where measured diffraction data can be used to construct a migration operator was formulated. The diffraction pattern can be measured using GPR with time-lapse acquisition. The time-lapse acquisition improves data quality considerably. The disturbance of the soil has a greater influence on the data than expected. The disturbed soil is probably responsible for the high energy-level in the top of the diffractor. Compared to the modeled impulse response, the amplitude versus offset in the tails of the diffractor decreases faster. The most likely causes for this effect are the finite aperture of the antennas and the attenuation in the soil. Both items are subject of further research with other models and measured data. These results suggest that using far field point source radiation patterns might not result in the optimal forward model for migration purposes. The disturbance of the soil is also subject of further research. In principle the diffracted data can now be used to improve the imaging operator

## Acknowledgements

This research is supported by the Dutch Technology Foundation.

## References

Berkhout, A., 1982, Seismic migration, imaging of acoustic energy by wave field extrapolation: Elsevier.

de Hoop, A., 1995, Handbook of radiation and scattering of waves: Academic Press.

Engheta, N., and Papas, C., November - December 1982, Radiation patterns of interfacial dipole antennas: Radio Science, **17**, no. 6, 1557–1566.

Gazdag, J., December 1978, Wave equation migration with the phase shift method: Geophysics, **43**, no. 7, 1342–1351.

van der Kruk, J., Wapenaar, C., and Fokkema, J., 2000, Multi-component 3-d imaging of ground penetrating radar data using matrix inversion in the spatial fourier domain: Proceedings Eight international conference on Ground-Penetrating Radar, Queensland, Australia, 508–513.

van der Kruk, J., Wapenaar, C., and Fokkema, J., 2001, Comparison of resolution functions of 3-d multi-component with 3-d single-component imaging algorithms for ground penetrating radar data: Proceedings 5th SEGJ International Symposium - Imaging Technology - The Society of Exploration Geophysicists of Japan (SEGJ), Tokyo, Japan, 229–236.

Wang, T., and Oristaglio, 2000, GPR imaging using the generalized radon transform.: Geophysics, **65**, no. 5, 1553–1559.

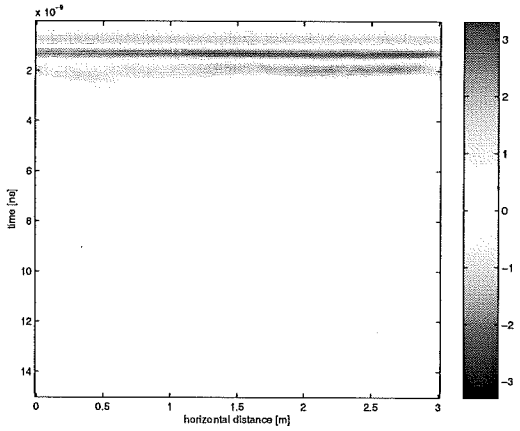


Fig. 2: Line of the data before an object was buried.

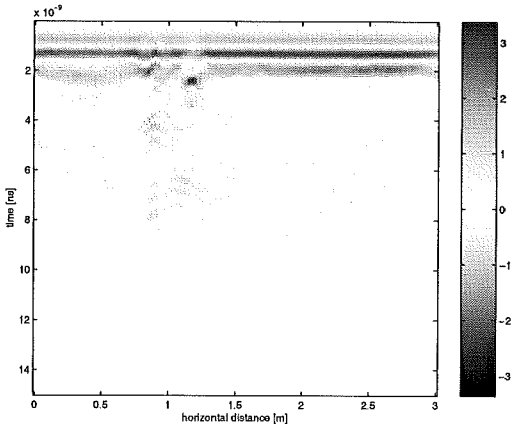


Fig. 3: Line of the data after an object was buried.

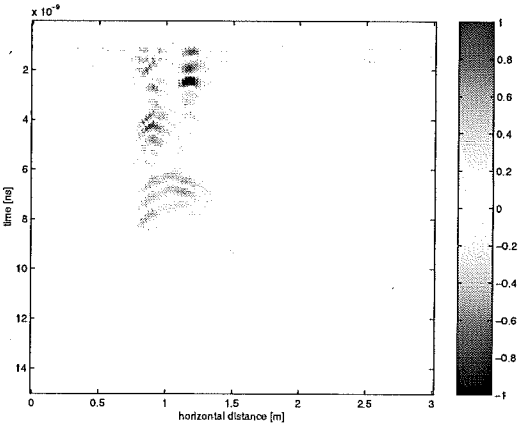


Fig. 4: Line of data when figure 2 is subtracted from figure 3.

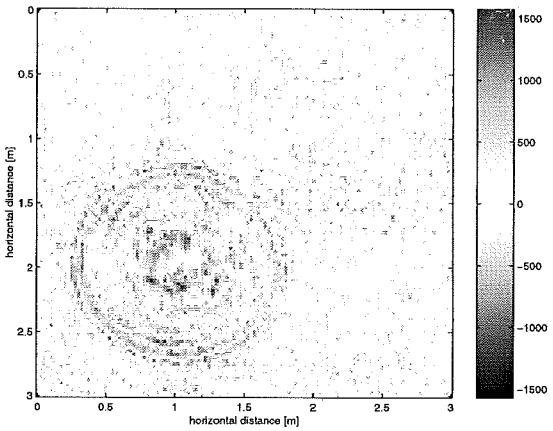


Fig. 5: Time slice of the subtracted data at 10 nanosec.

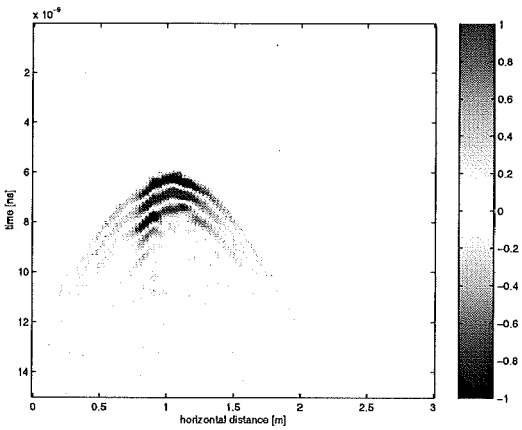


Fig. 6: The data from figure 4 with soil disturbance muted.

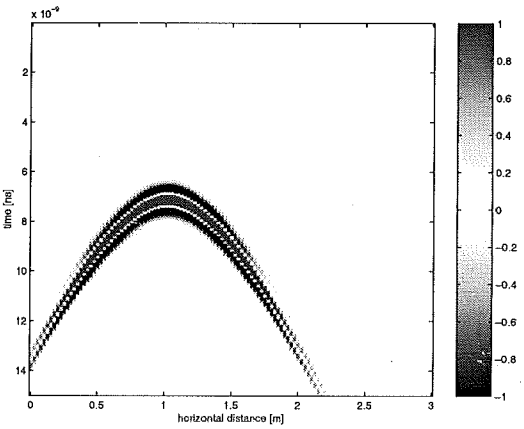


Fig. 7: Forward modeled with Engheta farfield.